Efficient four-wave mixing wavelength conversion in a hybrid silicon slot and polymer microring resonator

Hong, Jianxun
Wuhan University of Technology

Rokumyo, Kenta

Mao, Jiawei

Bannaron, Alisa

他

出版情報：Optics Express. 30 (25), pp.45499-, 2022-11-30. Optica Publishing Group
バージョン：

Research Article | Vol. 30, No. 25 / 5 Dec 2022 / Optics Express 45499
Optics EXPRESS

Efficient four-wave mixing wavelength conversion in a hybrid silicon slot and polymer microring resonator

JIANXUN HONG,[1,2] KENTA ROKUMYO,[3] JIAWEI MAO,[3] ALISA BANNARON,[1] HIROMU SATO,[1] AND SHIYOSHI YOKOYAMA[1,3,*]

[1]*Institute for Materials Chemistry and Engineering, Kyushu University, Kasuga, Fukuoka 816-8580, Japan*
[2]*School of Information Engineering, Wuhan University of Technology, Wuhan 430070, China*
[3]*Interdisciplinary Graduate School of Engineering Sciences, Kyushu University, Kasuga, Fukuoka 816-8580, Japan*
[*]*s_yokoyama@cm.kyushu-u.ac.jp*

Abstract: We present a silicon slot microring resonator for efficient frequency conversion via four-wave mixing (FWM). The slot consists of a narrow silicon waveguide pair with a gap of 80 nm, which is filled with a nonlinear optical polymer. The group velocity dispersion for the microring is controlled by engineering the geometry of the slot structure. Because of the large buildup factor of the slot microring, an FWM conversion efficiency of −27.4 dB is achieved with an optical pump power of less than 1.0 mW. From the measured power dependence of FWM generation, a nonlinear refractive index coefficient of 1.31×10^{-17} m^2 W^{-1} is obtained at a wavelength of 1562 nm. This work presents a hybrid silicon slot and polymer microring as a potential nonlinear device for applications in integrated photonic devices.

1. Introduction

Slot waveguides have a fundamental advantage for allowing a high degree of optical confinement, and thus provide unique optical properties in photonic applications when used as sub-micrometer-scale optical structures [1–3]. Characteristic performance can be observed in a silicon slot with a large difference in refractive index at the boundary of the high-refractive-index silicon region and a low-refractive-index dielectric region. In the simplest form of the silicon slot, two narrow silicon waveguides are separated by a distance of approximately 10 to 200 nm [4]. One of the propagating modes tends to confine the optical field with increased energy density within the slot, thereby resulting in a large overlap of the optical mode with the material filled in the gap. The inside of the low-index slot can be filled with various materials such as a metal oxide, gas, or polymer, enabling either light emission, sensing, or nonlinear optical properties [5–8].

In previous demonstrations, silicon-slot waveguides combined with nonlinear optical materials enabled efficient functionalities on small chips for opto-electric applications. One straightforward application is ultra-low-driving-voltage electro-optic modulators, which are fabricated by simply embedding electro-optic polymers within the slot [9,10]. Such material–waveguide hybridization is favorable in some electro-optic applications because silicon prohibits second-order nonlinear effects as a result of its centrosymmetric crystal structure. In contrast, silicon has intrinsic third-order nonlinearity that has been recognized as a promising property for all-optical switching and wavelength-conversion devices. Therefore, wavelength conversion and optical signal processing via the four-wave-mixing (FWM) process have been proposed for integrated silicon waveguides [11,12]. Nevertheless, the high degree of confinement in the silicon waveguide seriously limits the conversion efficiency and signal processing speed because of nonlinear losses, such as by two-photon-absorption-induced free-carrier absorption [13,14]. Solutions to the shortcomings that stem from the imperfect intrinsic material nature of silicon can be explored by combining

#475748 https://doi.org/10.1364/OE.475748
Journal © 2022 Received 14 Sep 2022; revised 12 Nov 2022; accepted 15 Nov 2022; published 30 Nov 2022

Optics EXPRESS

silicon waveguides with other optical materials. Silicon nitride, silicon-rich silicon oxide, hydrogen-terminated silicon, and chalcogenides have been investigated to compensate for the limited optical properties of silicon optical devices [15–18].

Organic compounds and polymers with large nonlinear refractive-index coefficients are also promising for overcoming the shortcomings of hybrid silicon slot waveguide devices. In particular, third-order nonlinear molecules that exhibit weak two-photon absorption and free-carrier absorption are promising for providing power-efficient wavelength conversion via the FWM process. In the present study, we fabricate a hybrid silicon slot and polymer microring resonator and demonstrate efficient nonlinear wavelength conversion. For a parametric process such as FWM, the group-velocity dispersion (GVD) is a critical parameter for attaining high-efficiency nonlinear conversion [19,20]. From this viewpoint, we extend the waveguide geometry of the silicon waveguide to the slot structure to optimize the FWM parameters. Because of the controlled reflective index profile across the high-refractive-index silicon region and the low-refractive-index polymer region, optical parameters such as the effective mode area [8,16], dispersion flatness, and zero-dispersion wavelength can be adjusted in the suitable silicon slot structure [21]. In Ref. [22], the strong interaction of the optical mode with the nonlinear optical compound can be seen in the straight silicon slot waveguide. A microring resonator designed with a small round-trip dispersion will support the phase-matching requirement, which is required for an efficient FWM generation. A dispersion-controlled microring was previously demonstrated in an FWM application using a horizontal slot waveguide filled with silicon nanocrystals [23,24]. Here, basing our device on the more common silicon-on-insulator (SOI) substrate, we designed an asymmetric slot in a waveguide to provide greater flexibility in tailoring the dispersion [25,26]. The microring is irradiated by pump and signal lasers at two different resonance wavelengths. The idler power generated via FWM is completely scaled by linear and quadratic trends against the signal and pump powers, respectively. The FWM conversion efficiency (CE) was −27.7 dB, with a pump power smaller than 1.0 mW. The obtained CE leads to a waveguide nonlinear parameter of 1034 W^{-1} m^{-1}, corresponding to a nonlinear refractive index of 1.31×10^{-17} m^2 W^{-1}. To the best of our knowledge, the efficiency of FWM and the measured nonlinear parameters are more than one order higher than the values reported for state-of-the-art microring devices based on nonlinear optical metal oxides and nitrides [27].

2. Hybrid silicon slot and polymer microring

2.1. Design and fabrication

A schematic showing an overview and cross-section of the microring is presented in Fig. 1(a). As the substrate, we used an SOI wafer with a 340-nm-thick silicon layer on a 3-μm-thick oxide layer. In the fabrication process, a 100-nm-thick SiO_2 film was deposited on top of the silicon layer as a mask to translate the waveguide and microring patterns using electron-beam lithography (ELS-G100, Elionix) and inductively coupled plasma etching (RIE-400iPB, SAMCO) using SF_6. The SiO_2 layer remained after etching was removed in dilute aqueous HF. A 10 wt% mixture of 1,4-bis[4-4(dimethylamino)phenyl]-1,3-butyldiene (BDPB) in polymethyl methacrylate was spin-coated from a cyclopentanone solution (5 wt%) to fill the slot area. An approximately 1.0-μm-thick film was obtained after the spin-coated film was dried at 95°C for 24 h. BDPB is an enhanced π-electron conjugated molecule that provides third-order nonlinear conversion in the fabricated microring via FWM [28,29]. The two-photon absorption maximum for BDPB appears at ~640 nm, which is much shorter than the FWM wavelength discussed in the present study. Thus, the two-photon absorption probability can be considered negligibly small.

For effective FWM generation, phase-matching in the waveguide should be satisfied, which requires a near-zero or small anomalous GVD to compensate for the nonlinear phase shift. Here, the GVD for the transverse electric (TE) mode in the silicon slot waveguides is characterized by finite element method (FEM) calculations. We use slot structures (Fig. 1(a)) having different

Optics EXPRESS

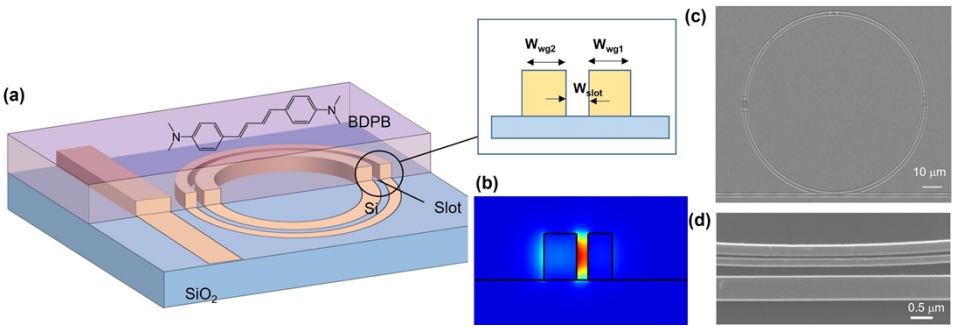

Fig. 1. Hybrid silicon slot and polymer microring. (a) Schematic and cross section of microring (not to scale). (b) Fundamental TE mode in slot ($W_{wg1} = 170$ nm, $W_{wg2} = 230$ nm, and $W_{slot} = 80$ nm). (c) SEM image of fabricated microring. (d) SEM image (magnified) of slot in microring coupled to waveguide.

cross-sections (W_{wg1} and W_{wg2}) and a constant W_{slot} of 80 nm, where $W_{wg1,2}$ and W_{slot} are the widths of the silicon waveguides and the slot distance, respectively. The calculated GVD, denoted as the dispersion parameter D, for the slot waveguides is shown in Fig. 2. The range of W_{wg1}/W_{wg2} provides GVD values from −1200 to 520 ps nm^{-1} km^{-1} at a wavelength of 1550 nm. Waveguides with large W_{wg1} and W_{wg2} (>280 nm) exhibit normal GVD. By comparison, waveguides with anomalous dispersion are allowed when the slots of the waveguides with W_{wg1} and W_{wg2} are smaller than 230 nm. For the silicon waveguides with $W_{wg1} = 230$ nm and $W_{wg2} = 230$ nm, the wavelength at zero dispersion is observed at 1535 nm and the GVD is 49 ps nm^{-1} km^{-1} at 1550 nm. Such an anomalous waveguide can be ideal for achieving phase matching for the FWM process. Nevertheless, the confinement in the slot becomes weak when the waveguide has a small bend, such as in the case of a microring resonator. To maintain a high degree of the confinement, the silicon slot is modified to be asymmetric [25,26]. The GVD for the asymmetric slot in waveguides with $W_{wg1} = 170$ nm and $W_{wg2} = 230$ nm are calculated and compared to the symmetric slot. The wavelength at zero dispersion is shifted to 1504 nm; thus, the anomalous dispersion is expanded by 30 nm compared with that for the symmetric slot. The mode calculation in Fig. 1(b) indicates a high degree of confinement in the designed slot. The mode confinement factor in the gap is 36.6%, which is defined as the ratio of the optical power trapped within the gap to the power for the entire waveguide. Thus, we chose the silicon slot of waveguides with $W_{wg1} = 170$ nm, $W_{wg2} = 230$ nm, and $W_{slot} = 80$ nm for fabrication. The bus waveguide has a width of 500 nm and supports a fundamental TE mode. It is noted that high-order modes attenuate quickly in the waveguide. Figures 1(c) and 1(d) show scanning electron microscopy (SEM; JSM-7000F, JEOL) images of the fabricated microring. In Fig. 1(c), a 50-μm-radius microring is coupled to the waveguide with a gap of 200 nm. The size parameters for the slot are $W_{slot} = 80 \pm 3$ nm, $W_{wg1} = 173 \pm 3$ nm, and $W_{wg2} = 230 \pm 3$ nm, which are confirmed by length measurement analysis of the fabricated microring in the magnified SEM image in Fig. 1(d).

2.2. Transmission spectrum and GVD

To measure the transmission spectrum of the microring resonator, we coupled TE polarized light from a tunable laser (Santec, TLS550) to the waveguide. The wavelength of the laser was swept with a step size of 1.0 pm, and the output power was recorded by a power monitor (Santec, MPM-210H). In Fig. 3(a), The transmission spectrum of the fabricated microring was recorded in the wavelength range from 1510 to 1610 nm. The beams were TE polarized using fiber polarization controllers and were coupled to the waveguide using a high-NA optical fiber. The transmission power in Fig. 3(a) is normalized to the maximum loss of about 8 dB

Optics EXPRESS

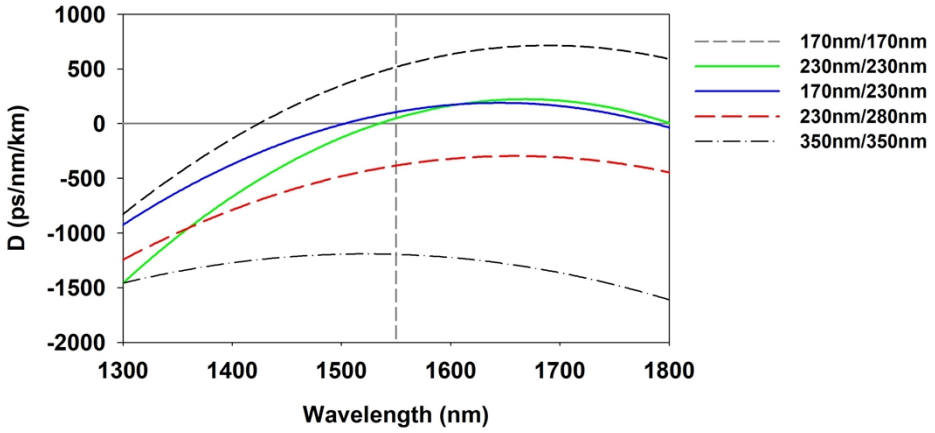

Fig. 2. Simulated GVD as a function of wavelength for silicon slots with various silicon widths. The slot distance is constant (80 nm).

which includes the 6.0 dB input and output coupling loss and 2 dB device insertion loss. To quantify the intrinsic quality factor and the propagation loss for the microring, we derived the transmission function from the recorded spectra using traveling wave theory [30]. According to the theoretical model, the fraction of laser coupling between the waveguide and the microring, and the fraction of propagation loss per round-trip in the microring, are defined as κ^2 and ${\kappa_p}^2$, respectively. The parameter κ^2 is the power coupling coefficient expressed as $\kappa^2 = \pi \times \delta\lambda \times (1 - \gamma^{1/2})/\mathrm{FSR}$, where $\delta\lambda$ is the −3 dB bandwidth, γ is the minimum power transmission, and FSR is the free-spectral range. The parameter ${\kappa_p}^2$ is the propagation loss coefficient expressed as ${\kappa_p}^2 = 2\pi \times \delta\lambda \times \gamma^{1/2}/FSR$. Using ${\kappa_p}^2$, we can express the propagation loss in the microring as $-10 \times \log(1 - {\kappa_p}^2)/L$ in units of dB cm^{-1}, where L is the microring perimeter. From the recorded transmission spectrum of the microring, the measured Q factor of 3500 is measured as $Q_t = \lambda_0/\delta\lambda = 2\pi\lambda_0/[\mathrm{FSR} \times (2\kappa^2 + {\kappa_p}^2)]$, whereas the intrinsic quality factor is derived as $Q_i = 2\pi\lambda_0/(\mathrm{FSR} \times {\kappa_p}^2) = Q_t/\gamma^{1/2}$. Taking one particular resonance at a wavelength of 1561.85 nm in Fig. 3(b), we obtain $\delta\lambda = 0.445$ nm and FSR = 8.91 nm. The extracted κ^2 and ${\kappa_p}^2$ values are 0.137 and 0.0395, respectively. Then, Q_i is determined to be 27,900, which corresponds to a propagation loss of 0.56 dB mm^{-1}. Compared to the symmetric slot in the straight line [22], rather lower loss is partially attributed to the asymmetric structure in which the field distribution of the optical mode is somewhat shifted into the wider silicon line. In calculations the losses of the bend slot waveguides with silicon widths of 170 nm/230 nm and 170 nm/170 nm are about 5.6 dB/cm and 13.9 dB/cm, respectively. The Q factors of the two designs are calculated to be 3500 and 3220, respectively by using the theoretical equation of single ring resonator [31]. It decreases by 8%. Note that, other parameter from the fitting results of Fig. 3(b) were used for calculations.

From the recorded transmission spectrum, the group index (n_g) and the GVD for the microring are characterized using the theoretical formulas $n_g = \lambda^2/(\mathrm{FSR} \times 2\pi R)$ and $D = (1/c)\mathrm{d}n_g/\mathrm{d}\lambda$, where R is the radius of the ring [20]. Figure 4 shows dispersion curves of n_g and D between 1510 and 1610 nm. The measured GVD for the microring is positive (i.e., the dispersion is anomalous), as expected from the estimated result. At a wavelength of ~1550 nm, the GVD is calculated to be 1100 ps nm^{-1} km^{-1}, which will result in a small round-trip dispersion (0.0033 ps nm^{-1}) and supports the phase-matching requirement as observed in the FWM property discussed in the next section. Note that, though tendency of the measured GVD to increase with increasing wavelength agrees with the calculated result, a difference occurs in the absolute values. This might be due to the structural imperfection of the fabricated slot.

Optics EXPRESS

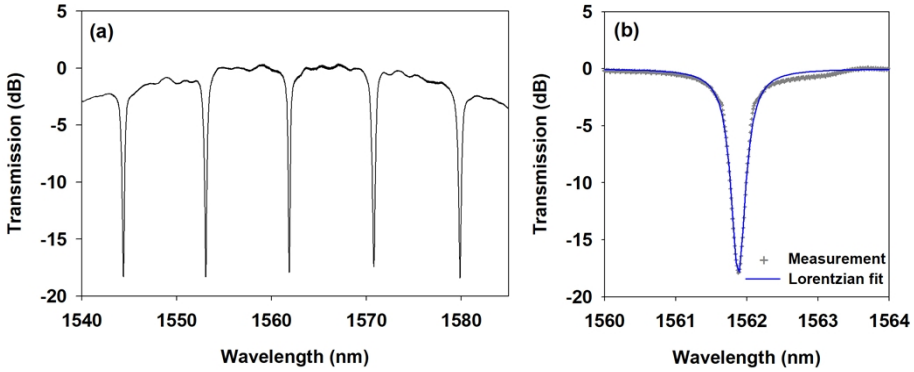

Fig. 3. (a) Transmission spectrum of microring. (b) Zoomed view of resonance peak at 1561.85 nm.

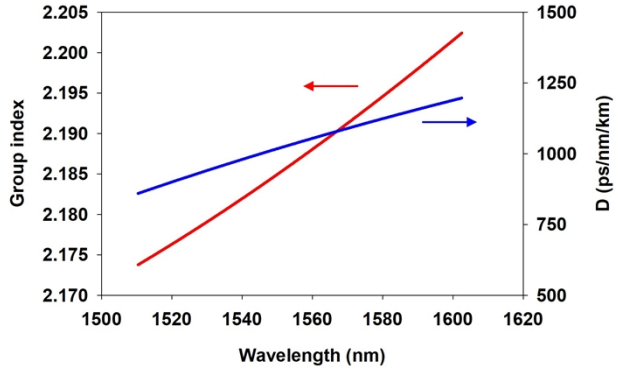

Fig. 4. Group index and GVD of hybrid silicon slot and polymer microring extracted from measured transmission spectrum.

2.3. Conversion via FWM

Figure 5(a) shows the experimental setup for acquiring the FWM spectra. Two tunable continuous-wave lasers were used, and one was connected to an erbium-doped fiber amplifier (EDFA) and filtered by a 1-nm tunable bandpass filter as the pump input. Another laser was used as the signal input and was combined with the pump input using a 50:50 coupler. The output light from the waveguide was conducted to an optical spectrum analyzer. The measured wavelength conversion via FWM can be found in the transmission spectrum shown in Fig. 5(b). The light power for the pump at 1561.85 nm and the signal at 1570.87 nm were 3 dBm and −15.6 dBm, respectively. The converted idler light was generated at 1552.97 nm, which was identical to a resonance wavelength of the microring. The conversion efficiency (η), defined as the power ratio between the output idler and the signal, is −27.4 dB. The intensity of the pump power was controlled lower than 3 dBm. Though a certain power handling should be concerned during the spectral measurement, the measured FWM spectra were stable with little degradation of the idler power under such pump power condition.

The relationship between the generated idler power and the input light power expected for the FWM process can be described by

$$P_{\mathrm{I}} = \left(\frac{16\gamma}{L}\right)^2 \left(\frac{Qc}{\omega_{\mathrm{P}} n_{\mathrm{g}}}\right)^4 P_{\mathrm{S}} P_P^2,$$

Optics EXPRESS

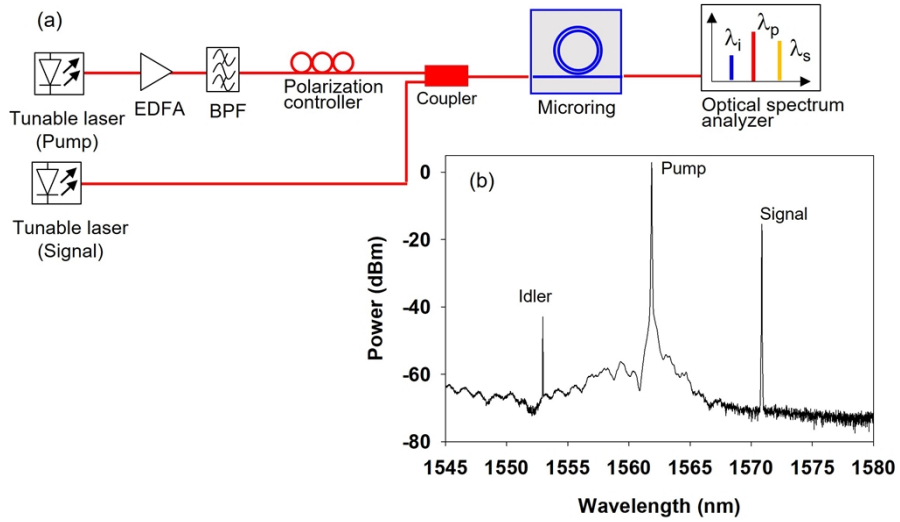

Fig. 5. (a) Experimental setup for FWM. EDFA: erbium-doped fiber amplifier, BPF: tunable bandpass filter. (b) Recorded FWM spectrum of hybrid slot and polymer microring.

where γ is the nonlinear waveguide parameter, c is the speed of light, ω_P is the frequency of the pump, and P_I, P_S, and P_P are the idler, signal, and pump light powers, respectively [30].

Figures 6(a) and 6(b) show the signal and pump power dependence of the generated idler power, respectively. The optical power is given in units of dBm. The circles and the solid lines represent the experimental data and linear fits to the data, respectively. The resultant linear fits give slopes of 1.00 and 1.98, which indicate linear and quadratic relationships between the input and idler powers, as expected for the FWM process. The relatively large conversion efficiency of the microring is attributed to the large third-order nonlinear optical efficiency of the molecules embedded in the silicon slot. The linear curves that well fit the measured data suggest negligible nonlinear losses from other nonlinear process such as two-photon absorption or free-carrier absorption. According to the mode calculation, the light is confined in the polymer in the gap of the slot structure, whereas only 18.4% of the total optical power propagates within the silicon. Hence, the slot mode is weakly affected by the nonlinear losses due to two-photon-absorption-induced free-carrier absorption [25].

The nonlinear parameter γ can be expressed as

$$\gamma = \left(\frac{\pi}{2}\right)^2 \frac{n_{gP}\sqrt{n_{gI}n_{gS}}}{\lambda_P\sqrt{\lambda_I\lambda_S}} \frac{L}{P_P Q_P \sqrt{Q_I Q_S}} \sqrt{\frac{P_I}{P_S}},$$

where λ_P is the pump wavelength [30,32]. Under the various FWM conditions used in Fig. 6(a) and 6(b), γ was calculated; the results are shown in Fig. 7. The mean value of γ was ~1034 W^{-1} m^{-1}, which is due to the sum of the material's nonlinear optical effect and mode confinement in the slot structure. The nonlinear refractive index (n_2) of the polymer can be estimated using the equation $n_2=\gamma c A_{eff}/\omega_P$. The A_{eff} is the effective mode area of the slot waveguide and calculated as 0.051 μm^{-2} according to the field profile of the fundamental mode [3,33]. Using the calculated A_{eff} and the measured γ value, we estimated a material's n_2 of 1.31×10^{-17} m^2 W^{-1}. The measured nonlinear refractive index is larger than those for silica, silicon, and other nonlinear optical waveguide materials such as SiN, ZnO, and AlN [34–36]. This result supports our expectation that the nonlinear material in the silicon slot provided fundamental advantages for building efficient functionalities on a small chip and exploring various nonlinear optical applications.

Optics EXPRESS

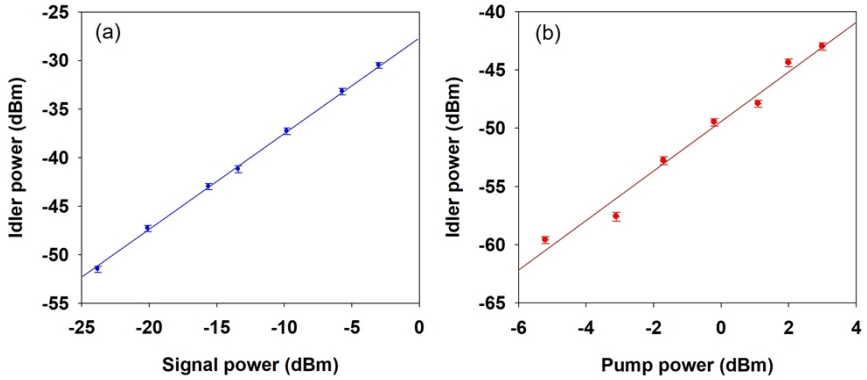

Fig. 6. Measured power for idler at different signal and pump powers. (a) Signal power is varied while pump power is constant at 3 dBm. The slope of the fitted line is 1.00. (b) Pump power is varied while signal power is constant at −15.6 dBm. The slope of the fitted line is 1.98.

Notably, the microring provides optical power magnification at the resonance, as described by the field enhancement factor. In the FWM process in the microring, the conversion efficiency is the product of the nonlinear waveguide parameter with an effective length and the buildup factor (F) for the resonance, as expressed by $\eta = P_I/P_s = |(2\pi n_2/\lambda A_{eff})\cdot P_P L_{eff}|^2 F^4$, where L_{eff} is the effective propagation length for the microring [26]. In our microring structure, we calculated L_{eff} of 118.5 mm and the buildup factor of ~10.7. The L_{eff} and buildup factor are influenced by the propagation loss, coupling coefficient, and phase mismatching. Therefore, further enhancement of the nonlinear optical response can be expected in the high-Q resonator while the light is circulating in the slot microring.

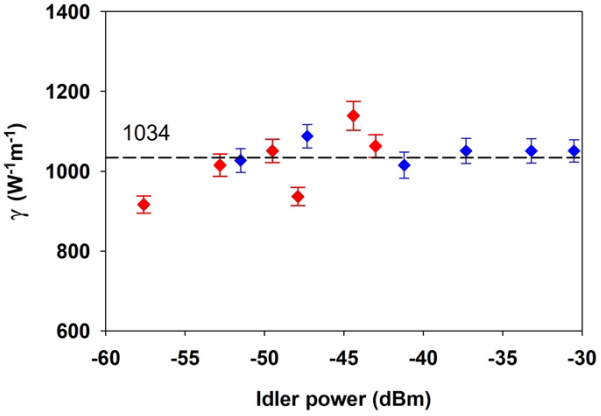

Fig. 7. Nonlinear parameter estimated using the theoretical equation. Blue and red squares correspond to experimental results in Figs. 6(a) and 6(b), respectively. The dashed horizontal line represents the mean γ value of 1034 W^{-1} m^{-1}.

3. Conclusion

A highly efficient FWM was experimentally demonstrated in a hybrid polymer–silicon compact slot microring resonator, with a Q factor of 3500 and a buildup factor of 10.7. The mode confinement in the silicon slot microring resonator exhibits strong interaction of the optical

Optics EXPRESS

field with the nonlinear polymer, which resulted in a larger effective length. From measured conversion efficiency, we obtained large nonlinear waveguide parameter, which enabled an efficient wavelength conversion of −27.4 dB with a low input pump power. The nonlinear waveguide parameter is 1034 W^{-1} m^{-1}, corresponding to a nonlinear refractive index of 1.31×10^{-17} m^2 W^{-1}.

Funding. Japan Society for the Promotion of Science (JP19H00770); Core Research for Evolutional Science and Technology (JPMJCR1674); National Institute of Information and Communications Technology (02101); Moonshot Research and Development Program (JPMJMS2063).

Acknowledgments. We wish to acknowledge the Cooperative Research Program of "Network Joint Research Center for Materials and Devices" and "Crossover Alliance to Create the Future with People, Intelligence, and Materials" of the Ministry of Education, Culture, Sports, Science and Technology of Japan.

Disclosures. The authors declare that there are no conflicts of interest related to this article.

Data availability. Data underlying the results presented in this paper are not publicly available at this time but may be obtained from the authors upon reasonable request.

References

1. R. Ding, T. Baehr-Jones, Y. Liu, R. Bojko, J. Witzens, S. Huang, J. Luo, S. Benight, P. Sullivan, J. M. Fedeli, M. Fournier, L. Dalton, A. Jen, and M. Hochberg, "Demonstration of a low VπL modulator with GHz bandwidth based on electro-optic polymer-clad silicon slot waveguides," Opt. Express **18**(15), 15618–15623 (2010).
2. Q. F. Xu, V. R. Almeida, R. R. Panepucci, and M. Lipson, "Experimental demonstration of guiding and confining light in nanometer-size low-refractive-index material," Opt. Lett. **29**(14), 1626–1628 (2004).
3. P. Sanchis, J. Blasco, A. Martinez, and J. Marti, "Design of silicon-based slot waveguide configurations for optimum nonlinear performance," J. Lightwave Technol. **25**(5), 1298–1305 (2007).
4. K. Debnath, A. Z. Khokhar, G. T. Reed, and S. Saito, "Fabrication of arbitrarily narrow vertical dielectric slots in silicon waveguides," IEEE Photonics Technol. Lett. **29**(15), 1269–1272 (2017).
5. Y. Y. Qiao, J. F. Tao, J. F. Qiu, X. B. Hong, and J. Wu, "Sensitive and ultrasmall sample volume gas sensor based on a sealed slot waveguide," Appl. Opt. **58**(17), 4708–4713 (2019).
6. M. Gould, T. Baehr-Jones, R. Ding, S. Huang, J. D. Luo, A. K. Y. Jen, J. M. Fedeli, M. Fournier, and M. Hochberg, "Silicon-polymer hybrid slot waveguide ring-resonator modulator," Opt. Express **19**(5), 3952–3961 (2011).
7. A. Martinez, J. Blasco, P. Sanchis, J. V. Galan, J. Garcia-Ruperez, E. Jordana, P. Gautier, Y. Lebour, S. Hernandez, R. Spano, R. Guider, N. Daldosso, B. Garrido, J. M. Fedeli, L. Pavesi, and J. Marti, "Ultrafast all-optical switching in a silicon-nanocrystal-based silicon slot waveguide at telecom wavelengths," Nano Lett. **10**(6), 2288 (2010).
8. R. Bhattacharjee, N. T. Kejalakshmy, and B. M. A. Rahman, "Design and optimization of an Al doped ZnO in Si-slot for gas sensing," IEEE Photonics J. **10**(4), 1–10 (2018).
9. S. Wolf, H. Zwickel, W. Hartmann, M. Lauermann, Y. Kutuvantavida, C. Kieninger, L. Altenhain, R. Schmid, J. D. Luo, A. K. Y. Jen, S. Randel, W. Freude, and C. Koos, "Silicon-organic hybrid (SOH) Mach-Zehnder modulators for 100 Gbit/s on-off keying," Sci. Rep. **8**(1), 2598 (2018).
10. C. Kieninger, Y. Kutuvantavida, D. L. Elder, S. Wolf, H. Zwickel, M. Blaicher, J. N. Kemal, M. Lauermann, S. Randel, W. Freude, L. R. Dalton, and C. Koos, "Ultra-high electro-optic activity demonstrated in a silicon-organic hybrid modulator," Optica **5**(6), 739–748 (2018).
11. M. A. Foster, A. C. Turner, J. E. Sharping, B. S. Schmidt, M. Lipson, and A. L. Gaeta, "Broad-band optical parametric gain on a silicon photonic chip," Nature **441**(7096), 960–963 (2006).
12. H. Fukuda, K. Yamada, T. Shoji, M. Takahashi, T. Tsuchizawa, T. Watanabe, J. Takahashi, and S. Itabashi, "Four-wave mixing in silicon wire waveguides," Opt. Express **13**(12), 4629–4637 (2005).
13. H. K. Tsang, C. S. Wong, T. K. Liang, I. E. Day, S. W. Roberts, A. Harpin, J. Drake, and M. Asghari, "Optical dispersion, two-photon absorption and self-phase modulation in silicon waveguides at 1.5 mu m wavelength," Appl. Phys. Lett. **80**(3), 416–418 (2002).
14. H. S. Rong, A. S. Liu, R. Nicolaescu, M. Paniccia, O. Cohen, and D. Hak, "Raman gain and nonlinear optical absorption measurements in a low-loss silicon waveguide," Appl. Phys. Lett. **85**(12), 2196–2198 (2004).
15. L. Razzari, D. Duchesne, M. Ferrera, R. Morandotti, S. Chu, B. E. Little, and D. J. Moss, "CMOS-compatible integrated optical hyper-parametric oscillator," Nat. Photonics **4**(1), 41–45 (2010).
16. X. Y. Wang, X. W. Guan, S. M. Gao, H. Hu, L. K. Oxenlowe, and L. H. Frandsen, "Silicon/silicon-rich nitride hybrid-core waveguide for nonlinear optics," Opt. Express **27**(17), 23775–23784 (2019).
17. F. Luan, M. D. Pelusi, M. R. E. Lamont, D. Y. Choi, S. Madden, B. Luther-Davies, and B. J. Eggleton, "Dispersion engineered As_2S_3 planar waveguides for broadband four-wave mixing based wavelength conversion of 40 Gb/s signals," Opt. Express **17**(5), 3514–3520 (2009).
18. K. Narayanan and S. F. Preble, "Optical nonlinearities in hydrogenated-amorphous silicon waveguides," Opt. Express **18**(9), 8998–9005 (2010).
19. A. C. Turner, C. Manolatou, B. S. Schmidt, M. Lipson, M. A. Foster, J. E. Sharping, and A. L. Gaeta, "Tailored anomalous group-velocity dispersion in silicon channel waveguides," Opt. Express **14**(10), 4357–4362 (2006).

Optics EXPRESS

20. E. Dulkeith, F. N. Xia, L. Schares, W. M. J. Green, and Y. A. Vlasov, "Group index and group velocity dispersion in silicon-on-insulator photonic wires," Opt. Express **14**(9), 3853–3863 (2006).
21. P. Muellner, M. Wellenzohn, and R. Hainberger, "Nonlinearity of optimized silicon photonic slot waveguides," Opt. Express **17**(11), 9282–9287 (2009).
22. C. Koos, P. Vorreau, T. Vallaitis, P. Dumon, W. Bogaerts, R. Baets, B. Esembeson, I. Biaggio, T. Michinobu, F. Diederich, W. Freude, and J. Leuthold, "All-optical high-speed signal processing with silicon–organic hybrid slot waveguides," Nat. Photonics **3**(4), 216–219 (2009).
23. L. Zhang, Y. Yue, Y. Y. Xiao-Li, J. Wang, R. G. Beausoleil, and A. E. Willner, "Flat and low dispersion in highly nonlinear slot waveguides," Opt. Express **18**(12), 13187–13193 (2010).
24. Q. A. Liu, S. M. Gao, Z. Q. Li, Y. Q. Xie, and S. L. He, "Dispersion engineering of a silicon-nanocrystal-based slot waveguide for broadband wavelength conversion," Appl. Opt. **50**(9), 1260–1265 (2011).
25. R. Ding, T. Baehr-Jones, W. J. Kim, B. Boyko, R. Bojko, A. Spott, A. Pomerene, C. Hill, W. Reinhardt, and M. Hochberg, "Low-loss asymmetric strip-loaded slot waveguides in silicon-on-insulator," Appl. Phys. Lett. **98**(23), 233303 (2011).
26. P. A. Anderson, B. S. Schmidt, and M. Lipson, "High confinement in silicon slot waveguides with sharp bends," Opt. Express **14**(20), 9197–9202 (2006).
27. C.-L. Wu, J.-Y. Huang, D.-H. Ou, T.-W. Liao, Y.-J. Chiu, M.-H. Shih, Y.-Y. Lin, A.-K. Chu, and C.-K. Lee, "Efficient wavelength conversion with low operation power in a Ta_2O_5-based micro-ring resonator," Opt. Lett. **42**(23), 4804–4807 (2017).
28. M. Albota, D. Beljonne, J. L. Bredas, J. E. Ehrlich, J. Y. Fu, A. A. Heikal, S. E. Hess, T. Kogej, M. D. Levin, S. R. Marder, D. McCord-Maughon, J. W. Perry, H. Rockel, M. Rumi, C. Subramaniam, W. W. Webb, X. L. Wu, and C. Xu, "Design of organic molecules with large two-photon absorption cross sections," Science **281**(5383), 1653–1656 (1998).
29. M. Rumi, J. E. Ehrlich, A. A. Heikal, J. W. Perry, S. Barlow, Z. Y. Hu, D. McCord-Maughon, T. C. Parker, H. Rockel, S. Thayumanavan, S. R. Marder, D. Beljonne, and J. L. Bredas, "Structure-property relationships for two-photon absorbing chromophores: bis-donor diphenylpolyene and bis(styryl)benzene derivatives," J. Am. Chem. Soc. **122**(39), 9500–9510 (2000).
30. S. J. Xiao, M. H. Khan, H. Shen, and M. H. Qi, "Compact silicon microring resonators with ultra-low propagation loss in the C band," Opt. Express **15**(22), 14467–14475 (2007).
31. H. Tazawa, Y.-h. Kuo, I. G. Dunayevskiy, J. Luo, A. K. Y. Jen, H. R. Fetterman, and W. H. Steier, "Ring resonator-based electrooptic polymer traveling-wave modulator," J. Lightwave Technol. **24**(9), 3514–3519 (2006).
32. A. Simbula, G. A. Rodriguez, M. Menotti, S. De Pace, S. M. Weiss, M. Galli, M. Liscidini, and D. Bajoni, "Low-power four-wave mixing in porous silicon microring resonators," Appl. Phys. Lett. **109**(2), 021106 (2016).
33. P. P. Absil, J. V. Hryniewicz, B. E. Little, P. S. Cho, R. A. Wilson, L. G. Joneckis, and P. T. Ho, "Wavelength conversion in GaAs micro-ring resonators," Opt. Lett. **25**(8), 554–556 (2000).
34. K. Ikeda, R. E. Saperstein, N. Alic, and Y. Fainman, "Thermal and Kerr nonlinear properties of plasma-deposited silicon nitride/silicon dioxide waveguides," Opt. Express **16**(17), 12987–12994 (2008).
35. E. Y. M. Teraoka, D. H. Broaddus, T. Kita, A. Tsukazaki, M. Kawasaki, A. L. Gaeta, and H. Yamada, "Self-phase modulation at visible wavelengths in nonlinear ZnO channel waveguides," Appl. Phys. Lett. **97**(7), 071105 (2010).
36. H. Jung, C. Xiong, K. Y. Fong, X. F. Zhang, and H. X. Tang, "Optical frequency comb generation from aluminum nitride microring resonator," Opt. Lett. **38**(15), 2810–2813 (2013).